arXiv:1606.06394v1 [cond-mat.mtrl-sci] 21 Jun 2016

Experimental and first-principles studies of magnetism and magnetoelectric effect in $Co_4Nb_2O_9$ and $Co_4Ta_2O_9$

I. V. Solovyev[1, 2, *] and T. V. Kolodiazhnyi[1]

[1] *National Institute for Materials Science, 1-1 Namiki, Tsukuba, Ibaraki 305-0044, Japan*

[2] *Department of Theoretical Physics and Applied Mathematics, Ural Federal University, Mira str. 19, 620002 Ekaterinburg, Russia*

(Dated: June 22, 2016)

Abstract

We report results of joint experimental and theoretical studies on magnetoelectric (ME) compounds $Co_4Nb_2O_9$ and $Co_4Ta_2O_9$. On the experimental side, we present results of the magnetization and dielectric permittivity measurements in the magnetic field. On the theoretical side, we construct the low-energy Hubbard-type model for the magnetically active Co3*d* bands in the Wannier basis, using the input of first-principles electronic structure calculations, solve this model in the mean-field Hartree-Fock approximation, and evaluate the electric polarization in terms of the Berry phase theory. Both experimental and theoretical results suggest that $Co_4Ta_2O_9$ is magnetically softer than $Co_4Nb_2O_9$. Therefore, it is reasonable to expect that the antiferromagnetic structure of $Co_4Ta_2O_9$ can be easier deformed by the external magnetic field, yielding larger polarization. This trend is indeed reproduced by our theoretical calculations, but does not seem to be consistent with the experimental behavior of the polarization and dielectric permittivity. Thus, we suggest that there should be a hidden mechanism controlling the ME coupling in these compounds, probably related to the magnetic striction or a spontaneous change of the magnetic structure, which breaks the inversion symmetry. Furthermore, we argue that unlike in other ME systems (e.g. Cr_2O_3), in $Co_4Nb_2O_9$ and $Co_4Ta_2O_9$ there are two crystallographic sublattices, which contribute to the ME effect. These contributions are found to be of the opposite sign and tend to compensate each other. The latter mechanism can be also used to control and reverse the electric polarization in these compounds.

I. INTRODUCTION

The exploration of magnetoelectric (ME) effect – the phenomenon, when the magnetization (electric polarization) can be induced by the external electric (magnetic) field – has attracted a great deal of attention, due to its potential applicability in the new generation of multifunctional electronic devises as well as in the fundamental studies, aiming at the search of new microscopic mechanisms of the ME coupling. Recently, the ME phenomenon is considered as a part of the more general paradigm called the 'multiferroism', where the appearance of spontaneous polarization is associated with some massive (and sometimes highly nontrivial) change of the magnetic structure.[1]

The canonical material exhibiting the ME effect is the rhombohedral Cr_2O_3, which was discussed by Dzyaloshinskii almost six decades ago.[2] Particularly, the antiferromagnetic structure, realized in Cr_2O_3, is such that the spacial inversion $\hat{I}$ enters the magnetic space group only in the combination with the time reversal $\hat{T}$. Therefore, the application of either electric or magnetic field, which destroys $\hat{I}$ or $\hat{T}$, respectively, will destroy also $\hat{I}\hat{T}$, thus, giving rise the electric polarization and the net magnetization. The symmetry properties of the induced electric polarization depend on other symmetry operations, but the existence of $\hat{I}\hat{T}$ is crucial for understanding the ME effect in Cr_2O_3.

The ME effect of a similar origin has been discovered by Fischer *et al.*[3] in 1972 in a family of $M_4A_2O_9$ materials, where M = Co or Mn and A = Nb or Ta. Like in Cr_2O_3, the magnetic structure of $M_4A_2O_9$ obeys the $\hat{I}\hat{T}$ symmetry, which can be destroyed by either electric or magnetic field. The interest to these materials has been recently revived in a series of papers which have addressed the details of the magnetic structure[4–7] and the ME coupling.[7–11]

For instance, with the availability of the single crystals it became possible to locate the easy axis for the magnetic moments[6] and to solve the magnetic structure of $Co_4Nb_2O_9$ in the $C2/c'$ magnetic space group[7] in contrast to the $P\bar{3}'c'1$ magnetic space group originally proposed by Bertaut et al.[4] Furthermore, as reported by Khan et al.,[7] ME tensor in $Co_4Nb_2O_9$ shows several off-diagonal components which implies the existence of toroidal moment.

So far no evidence of type-II multiferroism has been reported for $Co_4Ta_2O_9$ and $Co_4Nb_2O_9$ and these compounds have been classified as linear magnetoelectrics where an applied electric, E (magnetic, H) field induces magnetization, M (polarization, P).[7,9,10] In this contribution we report both experimental and first-principles analysis of the ME properties of

$Co_4Nb_2O_9$ and $Co_4Ta_2O_9$. Surprisingly, there is a significant difference in the magnitude of the ME effect in the $Co_4Nb_2O_9$ and $Co_4Ta_2O_9$ despite their identical crystal structure with the latter compound showing much weaker ME coupling at the Néel temperature, T_N. In accordance with a recent report by Xie et al.[12] we have detected a small anomaly in a zero-field dielectric permittivity at $T \leq T_N$ which confirms the magnetostriction effect in both compounds. We will try to rationalize some of these data using results of first-principles electronic structure calculations.

The rest of the article is organized as follows. In Sec. II we will present our experimental data for the magnetic (Sec. II A) and magnetodielectric (Sec. II B) properties of $Co_4Nb_2O_9$ and $Co_4Ta_2O_9$. Results of theoretical calculations will be discussed in Sec. III. Particularly, in Secs. III C and III D we will present our data, respectively, for the behavior of interatomic exchange interactions and the polarization in the magnetic field. Finally, in Sec. IV we discuss an overall picture emerging from the comparison of experimental and theoretical data and draw our conclusions.

II. EXPERIMENTAL RESULTS

Samples were prepared from 99.99% pure Co_3O_4, Nb_2O_5 and 99.9% pure Ta_2O_5. The stoichiometric mixtures were treated at 900–1000 °C for 10 h. Dense ceramic bodies were obtained by 10 h sintering in air at 1050 and 1300 °C for $Co_4Nb_2O_9$ and $Co_4Ta_2O_9$, respectively. Phase purity was confirmed by powder X-ray diffraction (MiniFlex600 diffractometer with Cu K_α x-ray source, Rigaku, Japan). Lattice parameters were obtained from Rietveld refinement of the X-ray data using JANA2006.[13] Magnetic susceptibility in the 2–100 K range was measured using superconducting quantum interference devise (Magnetic Property Measurement System, Quantum Design). For dielectric measurements, Au electrodes were spattered on the 1 mm thick disc-shaped ceramic samples. Dielectric properties in the 10 Hz – 1 MHz frequency range were measured with Novocontrol Alpha Impedance analyzer in the temperature interval of 2–40 K and magnetic fields up to 9 T. For temperature and magnetic field dependence of the dielectric properties we have used a home-made sample cell coupled with commercial cryostat equipped with superconducting magnet (Physical Property Measurement System, Quantum Design).

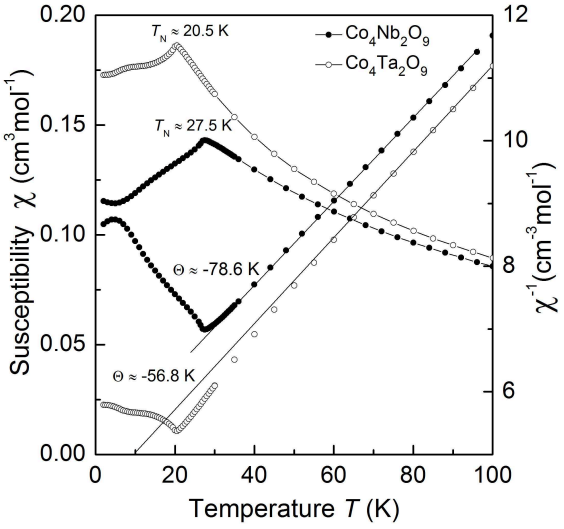

FIG. 1. Temperature dependence of magnetic susceptibility of $Co_4Nb_2O_9$ and $Co_4Ta_2O_9$.

A. Magnetic properties

Temperature dependence of magnetic susceptibility, χ, determined here as a ratio of magnetic moment, M, over magnetic field, H is shown in Fig. 1 together with inverse magnetic susceptibility for $Co_4Nb_2O_9$ and $Co_4Ta_2O_9$ powder samples measured at H = 50 Oe. The $\chi(T)$ shows a cusp at $T_N \approx 27.5$ and 20.5 K for $Co_4Nb_2O_9$ and $Co_4Ta_2O_9$, respectively, in agreement with literature data.[7,9,10] Below T_N the $\chi(T)$ decreases followed by a gradual increase at the lowest temperatures. This can be understood as an effect of anisotropic $\chi(T)$ behaviour as explained in detail in Refs. 6 and 7. The fit of inverse magnetic susceptibility to the Curie-Weiss law $\chi(T) = C/(T - \Theta)$, gives Weiss temperature of $\Theta \approx -78.6$ and -56.8 K and effective magnetic moments of $\mu_{eff} \approx 5.56$ and 5.36 μ_B for $Co_4Nb_2O_9$ and $Co_4Ta_2O_9$, respectively. The μ_{eff} of the title compounds are significantly larger than the spin-only effective magnetic moment of Co^{2+} $S = 3/2$ $\mu_{eff} = 3.87$ μ_B and indicate that orbital angular momentum is not quenched in the degenerate ground state, so there is significant contribution from the orbital angular magnetic moment.

Fig. 2 shows magnetic field dependence of Co^{2+} magnetic moment of the title compounds measured at 2 K. The change in the slope of the magnetization attributed to the spin-flop phase transition is detected at $\mu_0 H_c \sim 0.9$ T and ~ 0.5 T for $Co_4Nb_2O_9$ and $Co_4Ta_2O_9$, respectively. Clearly, $Co_4Ta_2O_9$ is magnetically softer than the $Co_4Nb_2O_9$. Please note

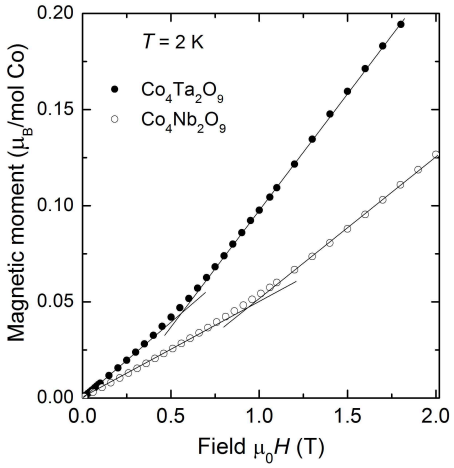

FIG. 2. Magnetic field dependence of magnetic moment of Co^{2+} ion in $Co_4Nb_2O_9$ and $Co_4Ta_2O_9$ measured at 2 K.

that our data on H_c refer to the 'average' critical field for polycrystalline materials. They are significantly larger than the $H_c \sim 0.2$ T measured along the easy plane $\boldsymbol{H}//x$ of the $Co_4Nb_2O_9$ single crystal. The orientation of the crystal is explained in Fig. 3. Note that in our notations x, y, and z correspond to, respectively, $[1\bar{1}0]$, $[\bar{1}\bar{1}0]$, and [001], in the notations of Ref. 7.

B. Magnetodielectric properties

Room temperature bulk resistivities of the title compounds are 3.3×10^5 and 4.4×10^4 Ω cm for $Co_4Nb_2O_9$ and $Co_4Ta_2O_9$, respectively. Therefore, the dielectric permittivity, ε', above 100 K is dominated by the Maxwell-Wagner effect due to the electrode and grain boundary polarization. Below ~ 50 K the free carriers are frozen in and dielectric properties are determined by the bulk of the crystals. The low-temperature dependence of the ε' and its first derivative measured at 0 T are shown in Fig. 4. An anomaly in the $\varepsilon'(T)$ dependence for both $Co_4Nb_2O_9$ and $Co_4Ta_2O_9$ is attributed to the antiferromagnetic (AFM) phase transition. This indicates a small but finite coupling of the spin ordering to the dielectric response in zero magnetic field in the title compounds. Note that earlier studies[8–10] could not detect the ME effect in $Co_4Nb_2O_9$ and $Co_4Ta_2O_9$ at zero magnetic field. Very recently magnetoelastic coupling was proposed in $Co_4Nb_2O_9$ based on the anomaly in the lattice strain below T_N.[12] Magnetoelastic contraction of the lattice can be partially responsible for

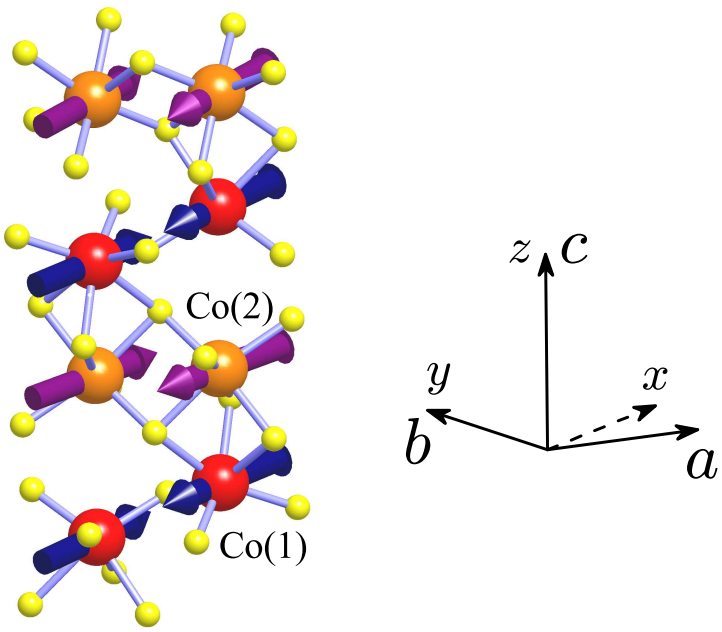

FIG. 3. (Color online) Fragment of the crystal and magnetic structure of $Co_4Nb_2O_9$ in the ground state. The relative orientation of hexagonal (a, b, and c) and cartesian (x, y, and z) axes is explained on the right.

a notable upturn in the $\varepsilon'(T)$ below T_N in both compounds shown in Fig. 4a in which case one would expect slight re-normalization of the phonon frequencies due to the spin-phonon coupling. This conclusion is supported by the absence of the frequency dispersion of the dielectric permittivity below Néel temperature reported in literature[12] and also confirmed in this work.

In contrast to our expectations, the two title compounds show quantitatively different magnetocapacitance effect. The effect of magnetic field on the scaled dielectric permittivity with subtracted zero-field background, $\Delta\varepsilon'/H^2 = (\varepsilon'(H) - \varepsilon'(H = 0))/H^2$, versus $T - T_N$ is shown in Figure 5. According to our data, at 1 T the $\Delta\varepsilon'/H^2$ value at T_N is ~ 4 times higher for $Co_4Nb_2O_9$ than for $Co_4Ta_2O_9$. The difference increases to ~ 88 at magnetic field of 7 T. Magnetic-field induced spontaneous polarization, P, for polycrystalline $Co_4Nb_2O_9$ and $Co_4Ta_2O_9$ reported in the literature[9,10] equal to $P \approx 120$ μC/m^2 and 44 μC/m^2 at 7 T, respectively. Because the dielectric susceptibility at the phase transition is equal to the induced polarization response to a small electric stimuli, the factor of 2.7 difference in P is in reasonable agreement with a factor of 4 difference in mangetocapacitance at low magnetic

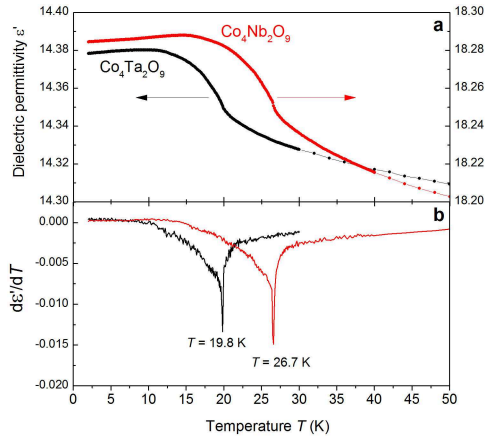

FIG. 4. Zero field dielectric permittivity (a) and its temperature derivative (b) for $Co_4Nb_2O_9$ and $Co_4Ta_2O_9$ measured at 250 kHz.

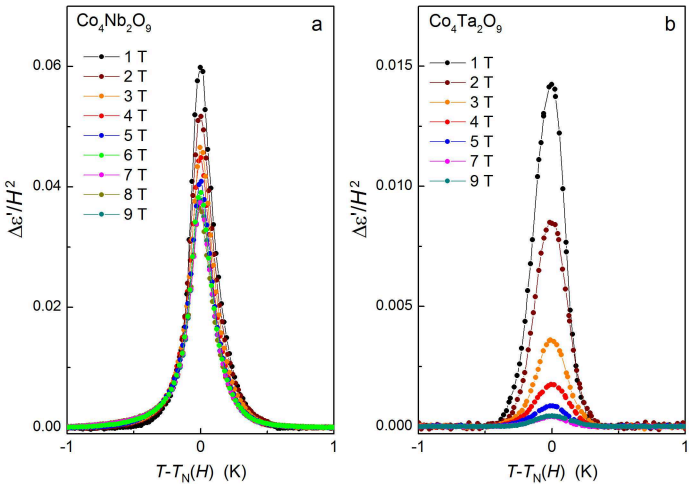

FIG. 5. Scaled dielectric permittivity with subtracted zero-field background, $(\varepsilon'(H) - \varepsilon'(H = 0))/H^2$, versus $T - T_N$. Dielectric permittivity was measured at 1 kHz.

field.

According to the model developed for linear magnetoelectric, e.g., $MnTiO_3$,[14] the $\Delta\varepsilon'$ is expected to scale linearly with H^2 which should yield a field-independent value of the $\Delta\varepsilon'/H^2$ maximum. As evidenced from the Fig. 6 this is not exactly the case for $Co_4Nb_2O_9$ and $Co_4Ta_2O_9$. The $\Delta\varepsilon'/H^2$ shows a notable decrease with increasing magnetic field before it levels off at $\mu_0 H \geq 7$ and 5 T for $Co_4Nb_2O_9$ and $Co_4Ta_2O_9$, respectively. The saturation of the $\Delta\varepsilon'/H^2$ maximum is difficult to attribute to the spin flop phase transition because the

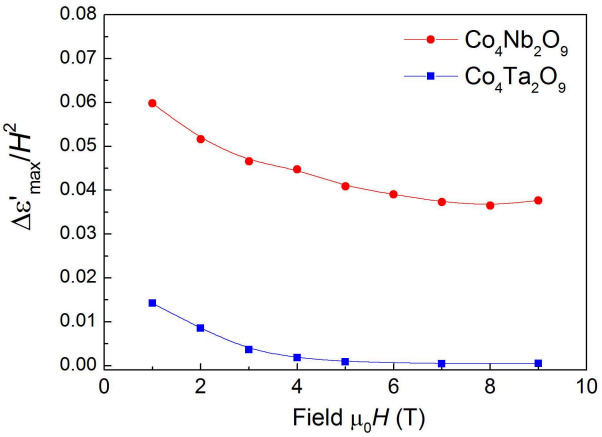

FIG. 6. Magnetic field dependence of the maximum of the scaled dielectric permittivity at $T_{\rm N}$.

$\Delta\varepsilon'/H^2$ saturation occurs at the fields significantly higher than the spin flop critical fields $\mu_0 H_c$ of less than 1 T for both compounds. To gain further insight into the origin of the ME effect below we report the results of the first-principles calculations.

III. THEORETICAL CALCULATIONS

A. Main details of crystal and electronic structure

$Co_4Nb_2O_9$ and $Co_4Ta_2O_9$ crystallize in the centrosymmetric trigonal $P\overline{3}c1$ structure (No. 165). The fragment of this structure is shown in Fig. 3. There are two inequivalent types of Co atoms, alternating along the z axis and forming the (distorted) honeycomb layers in the xy-plane. In our electronic structure calculations, we use the experimental room-temperature atomic positions and lattice parameters, reported in Refs. 15 and 16 for $Co_4Nb_2O_9$ and $Co_4Ta_2O_9$, respectively. The total and partial densities of states, obtained in the local-density approximation (LDA), are explained in Fig. 7. The states located near the Fermi level are the Co3d bands, which in the octahedral CoO_6 environment are split into lower-energy t_{2g} and higher-energy e_g bands. These bands are mainly responsible for the magnetic properties of $Co_4Nb_2O_9$ and $Co_4Ta_2O_9$. Regarding the LDA band structure, there are two main differences between $Co_4Nb_2O_9$ and $Co_4Ta_2O_9$. The Ta5d states are considerably more extended in comparison with the Nb4d ones, and, therefore, much stronger hybridize with the O2p states. This explains the additional upward shift of the antibonding

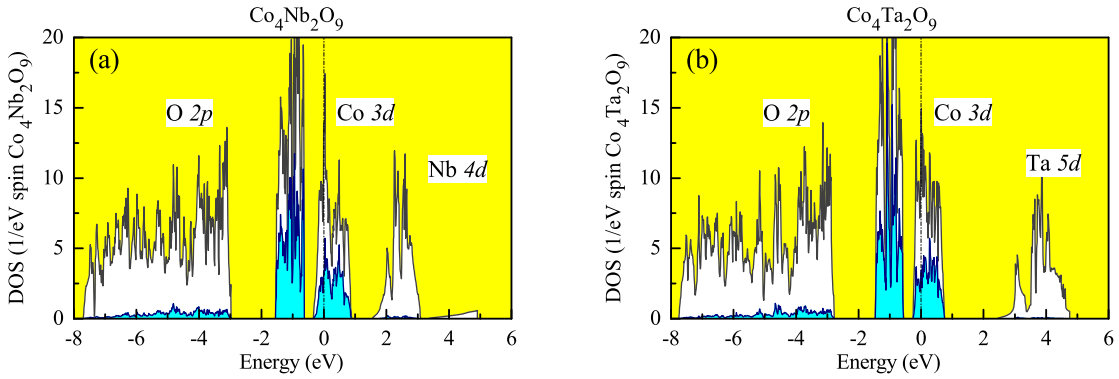

FIG. 7. (Color online) Total and partial densities of states of $Co_4Nb_2O_9$ and $Co_4Ta_2O_9$ in the local density approximation. The shaded light (blue) area shows contributions of the Co3d states. Positions of the main bands are indicated by symbols. The Fermi level is at zero energy (shown by dot-dashed line).

Ta5d band, arising from the O2p-Ta5d hybridization. This in turn reduces the Co3d-Ta5d hybridization and slightly decreases the width of the Co3d bands in $Co_4Ta_2O_9$. In this sense, the Co3d states in $Co_4Ta_2O_9$ are slightly more "localized" in comparison with $Co_4Nb_2O_9$.

B. The effective low-energy electron model

In this section, we briefly remind the reader the main steps of the construction and solution of the effective low-energy model, which is used for the analysis of electronic and magnetic properties of $Co_4Nb_2O_9$ and $Co_4Ta_2O_9$.

The first step of our approach is the construction of the effective Hubbard-type model for the magnetically active Co3d bands:

$$\hat{\mathcal{H}} = \sum_{ij}\sum_{\sigma\sigma'}\sum_{ab}\left(t_{ab}^{ij}\delta_{\sigma\sigma'} + \Delta t_{ab}^{i\sigma\sigma'}\delta_{ij}\right)\hat{c}_{ia\sigma}^{\dagger}\hat{c}_{jb\sigma'} + \frac{1}{2}\sum_{i}\sum_{\sigma\sigma'}\sum_{abcd}U_{abcd}^{i}\hat{c}_{ia\sigma}^{\dagger}\hat{c}_{ic\sigma'}^{\dagger}\hat{c}_{ib\sigma}\hat{c}_{id\sigma'}, \qquad (1)$$

starting from the electronic band structure in LDA. The model itself is formulated in the basis of Wannier functions, which were obtained using the projector-operator technique (Refs. 17 and 18) and the orthonormal linear muffin-tin orbitals (LMTO's, Ref. 19) as the trial wave functions. $\sigma(\sigma')=\uparrow$ or $\downarrow$ in (1) are the spin indices, while a, b, c, and d label five 3d orbitals. The parameters of the one-electron part, $\hat{t} = [t_{ab}^{ij}]$, are defined as the matrix elements of the LDA Hamiltonian in the Wannier basis.[17] $\Delta\hat{t} = [\Delta t_{ab}^{i\sigma\sigma'}]$ is the

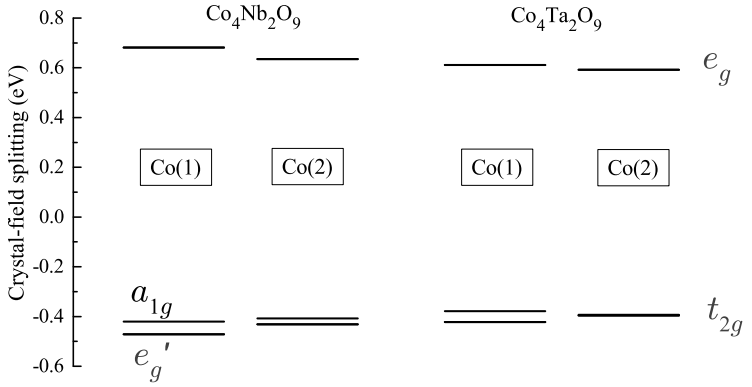

FIG. 8. Scheme of the crystal-field splitting for two inequivalent Co sites in $Co_4Nb_2O_9$ and $Co_4Ta_2O_9$.

matrix of spin-orbit (SO) interaction, also in the Wannier basis. The parameters of screened on-site Coulomb interactions, $\hat{U} = [U^i_{abcd}]$, are calculated in the framework of constrained random-phase approximation (RPA),[20] using the simplified procedure, which was explained in Ref. 17.

The crystal-field splitting, obtained from the diagonalization of the site-diagonal part of $\hat{t}$, is shown in Fig. 8. One can clearly see that the main effect is the t_{2g}-e_g splitting in the octahedral CoO_6 environment. Other splittings are considerably smaller. For instance, three t_{2g} levels are split into lower-energy doublet (e'_g) and higher-energy singlet (a_{1g}), being consistent with the d^7 configuration of Co^{2+}, where two minority-spin electrons are accommodated in the lower-energy doublet. The largest splitting of the t_{2g} levels is about 50 meV, which is comparable with the strength of the SO coupling ξ (about 75 meV). Thus, one can expect the existence of unquenched orbital magnetization, which is supported by the experimental susceptibility data.

Each 5×5×5×5 matrix $\hat{U} = [U^i_{abcd}]$ can be parameterized in terms of three parameters: the Coulomb repulsion $U = F^0$, the intraatomic exchange interaction $J = (F^2+F^4)/14$, and the 'nonsphericity' $B = (9F^2-5F^4)/441$, where F^0, F^2, and F^4 are the screened radial Slater's integrals. The results of such parametrization are shown in Table I. The parameters U are generally larger in $Co_4Ta_2O_9$. This is due to the additional energy separation between the Co3d and Ta5d bands (see Fig. 7), which results in less efficient screening of the Coulomb interactions in the Co3d band by the Ta5d band.[17] Moreover, due to different crystallographic

TABLE I. Parameters of screened Coulomb interaction (U), exchange interaction (J) and non-sphericity (B) for the inequivalent Co sites in $Co_4Nb_2O_9$ and $Co_4Ta_2O_9$ (in eV).

	$Co_4Nb_2O_9$		$Co_4Ta_2O_9$	
	Co(1)	Co(2)	Co(1)	Co(2)
U	2.95	3.00	3.00	3.29
J	0.94	0.93	0.94	0.95
B	0.10	0.10	0.10	0.10

environment, the Coulomb U is different for the Co sites 1 and 2, and this difference is substantially larger in $Co_4Ta_2O_9$.

Other parameters of the model Hamiltonian can be found elsewhere.[21]

C. Magnetic interactions and magnetic ground state

After the construction, the model was solved in the mean-field Hartree-Fock approximation.[17] Then, the isotropic exchange interactions can be evaluated by considering the infinitesimal rotations of spins and mapping corresponding energy changes onto the spin Heisenberg model $E_{\rm H} = -\sum_{i>j} J_j \boldsymbol{e}_i \cdot \boldsymbol{e}_{i+j}$, where $\boldsymbol{e}_i$ denotes the *direction of spin* at the site i.[22]

We have found that the lowest energy corresponds to the AFM ground state, where all the spins are coupled ferromagnetically along the z axis and antiferromagnetically in the xy plane (see Fig. 3), being in total agreement with the experimental data.[7,9] The corresponding electronic structure is shown in Fig. 9. The $3d$ states in $Co_4Nb_2O_9$ and $Co_4Ta_2O_9$ are indeed well localized: the atomic levels are split by large crystal field and on-site Coulomb interactions. The interatomic transfer integrals are considerably weaker and lead to the formation of narrow bands around the atomic levels. The main difference between $Co_4Nb_2O_9$ and $Co_4Ta_2O_9$ is the additional upward shift of the Co(2) states in the latter compound due to larger Coulomb repulsion (see Table I). In particular, it reduces the band gap in $Co_4Ta_2O_9$, which is formed between minority-spin states of the atoms Co(2) and Co(1).

The obtained type of the magnetic ground state can be easily understood by considering the behavior of interatomic exchange interactions (Fig. 10). One can see that the main in-

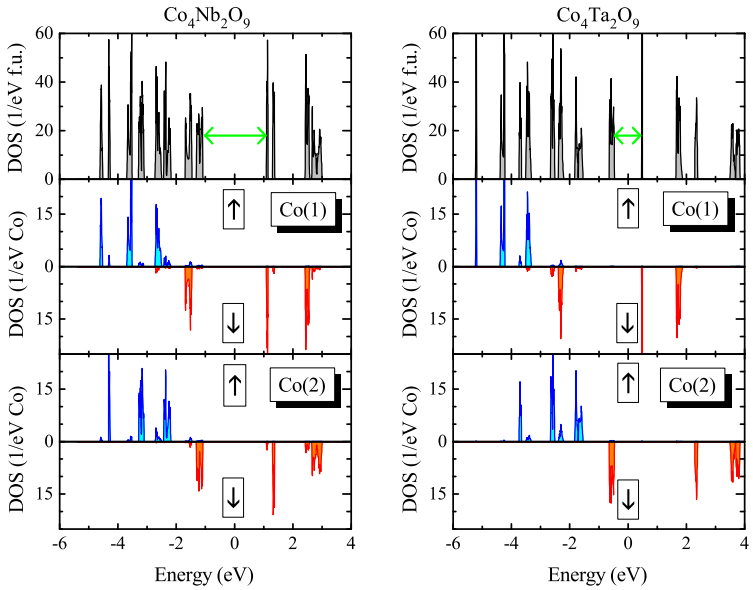

FIG. 9. (Color online) Total and partial densities of states for the two inequivalent Co-sites in $Co_4Nb_2O_9$ and $Co_4Ta_2O_9$, as obtained in the model Hartree-Fock calculations for the antiferromagnetic ground state. The green arrows show the band gap, which is formed between states of the inequivalent Co-atoms. The Fermi level is at zero energy.

teractions are AFM. Partly, this is an artifact of our model analysis, because it does not take into account the polarization of the O2p states, which gives rise to important ferromagnetic (FM) contributions to the exchange coupling. For instance, the Néel temperature, estimated using the calculated parameters is about 170 K and 100 K for $Co_4Nb_2O_9$ and $Co_4Ta_2O_9$, respectively. It is strongly overestimated in comparison with the experimental data (27.5 K and 20.5 K for $Co_4Nb_2O_9$ and $Co_4Ta_2O_9$, respectively). This overestimation is partly caused by the mean-field approximation. However, there is also an intrinsic error, inherent to the low-energy model itself, which does not take into account the FM contributions caused by the polarization of the O2p states. Similar overestimation has been found for the Weiss temperature (-255 K and -155 K, for $Co_4Nb_2O_9$ and $Co_4Ta_2O_9$, respectively). We would like to note that this problem is not new and was also encountered in other systems, which are close to the charge transfer regime, and where the oxygen states play a more important role and, as a rule, should be explicitly treated in the model analysis.[23,24] The correct quantitative description is possible by considering the direct exchange interactions and the magnetic polarization of the O2p band.[24] Nevertheless, the magnetic interactions, obtained

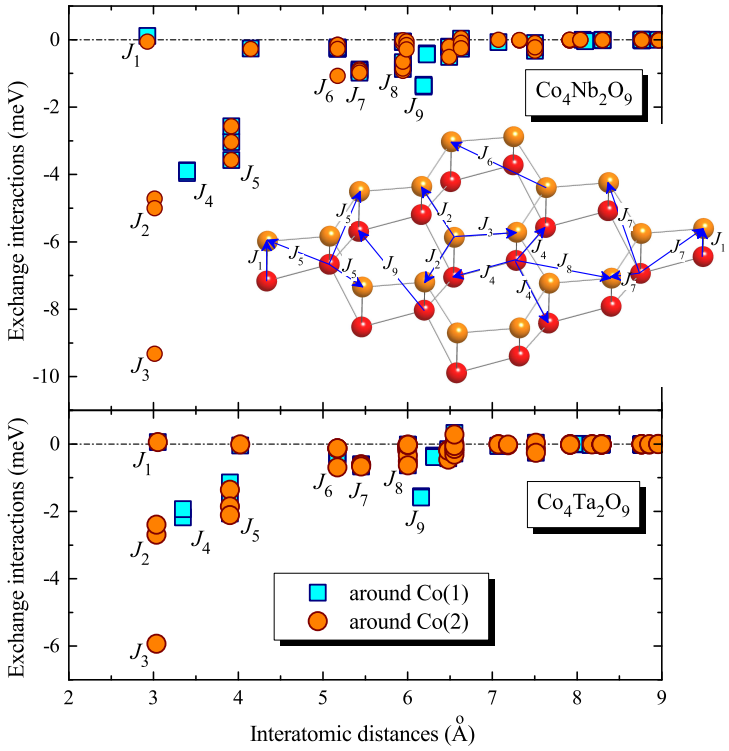

FIG. 10. (Color online) Distance dependance of interatomic exchange interactions in $Co_4Nb_2O_9$ and $Co_4Ta_2O_9$ around two inequivalent types of Co atoms. The main exchange interactions are explained in the inset, where the Co-atoms of the first and second types are shown by darker (red) and lighter (orange) spheres, respectively.

in the present low-energy model, are well consistent with the observed AFM ground state: the main interactions, stabilizing the AFM alignment in the xy plane, are J_2, J_3, and J_4. In the combination with the AFM interaction J_5, they also stabilize the FM alignment along z. The AFM interactions are systematically weaker in $Co_4Ta_2O_9$ (and, therefore, magnetically this system is expected to be softer). This is consistent with somewhat narrower Co3d bandwidth (Fig. 7), larger values of U, which weakens the superexchange interactions, and also smaller bandgap between the minority-spin states, which enlarges the FM contributions to the superexchange coupling.[25]

After turning on the SO coupling, the magnetic moments become aligned mainly in the xy plane. In this case, we have found two nearly degenerate solutions with the magnetic moments being mainly parallel to either x or y axes and obeying the following symmetries

(the magnetic space groups), respectively, $\boldsymbol{G}_1 = \{\hat{E}, \hat{T}\hat{I}, \hat{T}\hat{m}_y, \hat{C}_y^2\}$ (or $C2/c'$ in the notations of Ref. 7) and $\boldsymbol{G}_2 = \{\hat{E}, \hat{T}\hat{I}, \hat{m}_y, \hat{T}\hat{C}_y^2\}$, where $\hat{E}$ is the unity operation, $\hat{I}$ is the inversion, $\hat{m}_y$ and $\hat{C}_y^2$ are, respectively, the mirror reflection and the 180° rotation about the y axis, combined with the half of the hexagonal translation, $\boldsymbol{c}/2$, and $\hat{T}$ is the time inversion operation. The threefold rotation about the z (c) axis, which is the symmetry operation of the parent space group $P\overline{3}c1$, is forbidden by the magnetic alignment in the xy plane. The first such solution is illustrated in Fig. 3. Both in $\boldsymbol{G}_1$ and $\boldsymbol{G}_2$, the magnetic moments exhibit the AFM canting out of the main (either x or y) axis due to the joint effect of the single-ion anisotropy and Dzyaloshinskii-Moriya interactions. The canting angle at the site Co(1) and Co(2) in $Co_4Nb_2O_9$ ($Co_4Ta_2O_9$) is about 2° (1°) and 6° (7°), respectively. This canting is considerably smaller than the experimental one,[7] due to the overestimation of isotropic exchange interactions in the low-energy model, which makes these magnetic materials substantially harder than in the experiment. Moreover, we have found an appreciable orbital contribution, which constitutes about 17-20% of the total magnetization at the Co site in the ground state.

D. Magnetic-field dependence of electric polarization

The electronic polarization in the external magnetic field can be computed in the reciprocal space, using the formula of King-Smith and Vanderbilt:[26]

$$\mathbf{P} = -\frac{ie}{(2\pi)^3} \sum_n \int_{BZ} d\mathbf{k} \, \langle u_{n\mathbf{k}} | \partial_{\mathbf{k}} u_{n\mathbf{k}} \rangle, \tag{2}$$

where $u_{n\mathbf{k}}(\mathbf{r}) = e^{-i\mathbf{kr}}\psi_{n\mathbf{k}}(\mathbf{r})$ is the cell-periodic eigenstate of the model Hamiltonian $H_{\mathbf{k}} = e^{-i\mathbf{kr}} H e^{i\mathbf{kr}}$, which in our case is treated in the Hartree-Fock (HF) approximation, the summation runs over the occupied bands (n), the $\mathbf{k}$-space integration goes over the first Brillouin zone (BZ), and $-e$ ($e > 0$) is the electron charge. Since the Co3d states in $Co_4Nb_2O_9$ and $Co_4Ta_2O_9$ are well localized (see Fig. 9), the analysis can be also performed in the real space, starting from the limit of atoms states and using the perturbation theory expansion with respect to the transfer integrals.[27]

Since $\hat{T}\hat{I}$ is one of the symmetry operations in $\boldsymbol{G}_1$ and $\boldsymbol{G}_2$, these states develop neither spontaneous polarization $\mathbf{P}$ nor the net magnetization $\mathbf{M}$. However, both polarization and magnetization can be induced by the magnetic field, which breaks $\hat{T}\hat{I}$.[2] When applied along

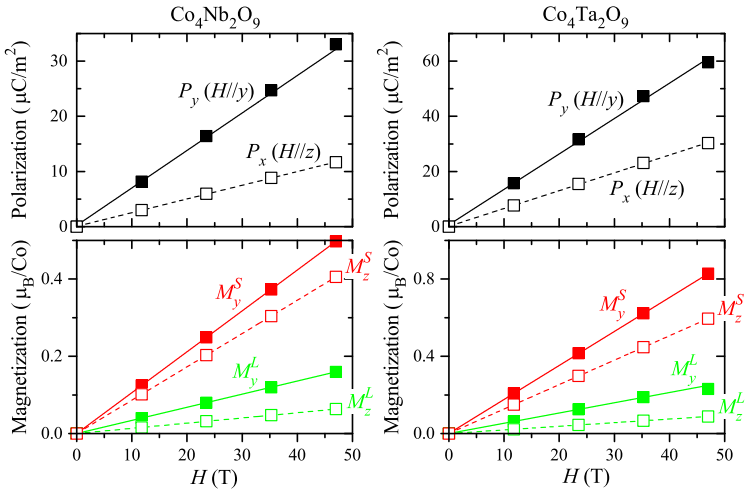

FIG. 11. (Color online) Nonvanishing components of electric polarization (P) and the net spin (M^S) and orbital (M^L) magnetization as obtained in the model Hartree-Fock calculations for the $\boldsymbol{G}_1$ state in the magnetic field being parallel to either y or z axes.

the x, y, or z axis in the $\boldsymbol{G}_1$ state it, respectively, causes the spin-flop transition to the $\boldsymbol{G}_2$ state, breaks the $\hat{T}\hat{m}_y$ symmetry (while the symmetry operation $\hat{C}_y^2$ remains) and induces the polarization parallel to the y axis, and breaks the $\hat{C}_y^2$ symmetry (while $\hat{T}\hat{m}_y$ remains) and induces the polarization in the zx plane. Moreover, we have found that the z component of the electric polarization is negligibly small, which is consistent with the experimental data.[7] The results of numerical simulations are presented in Fig. 11. In the $\boldsymbol{G}_2$ state, the magnetic field applied along either x or z axes, breaks the $\hat{m}_y$ symmetry (while the symmetry operation $\hat{T}\hat{C}_y^2$ remains) and induces the electric polarization parallel to the y axis (Fig. 12). The magnetic field along the y axis causes the spin-flop transition to the $\boldsymbol{G}_1$ state. The toroidal moment $\mathbf{T} \sim (\mathbf{P} \times \mathbf{M})$ is expected in the $\boldsymbol{G}_1$ state when $\boldsymbol{H}//z$ and in the $\boldsymbol{G}_2$ state when $\boldsymbol{H}//x$ or z.[7]

The calculated polarization is generally larger in $Co_4Ta_2O_9$. This is because of two factors. On the one hand, $Co_4Ta_2O_9$ is magnetically softer than $Co_4Nb_2O_9$ and, therefore, the magnetic structure of $Co_4Ta_2O_9$ can be easier deformed by the magnetic field. This effect alone nicely explains the behavior of the electric polarization, when the magnetic field is applied in the xy plane: the dependence of P_y on the total (spin plus orbital) net magnetization is practically identical for $Co_4Nb_2O_9$ and $Co_4Ta_2O_9$ (see Fig. 13). Therefore,

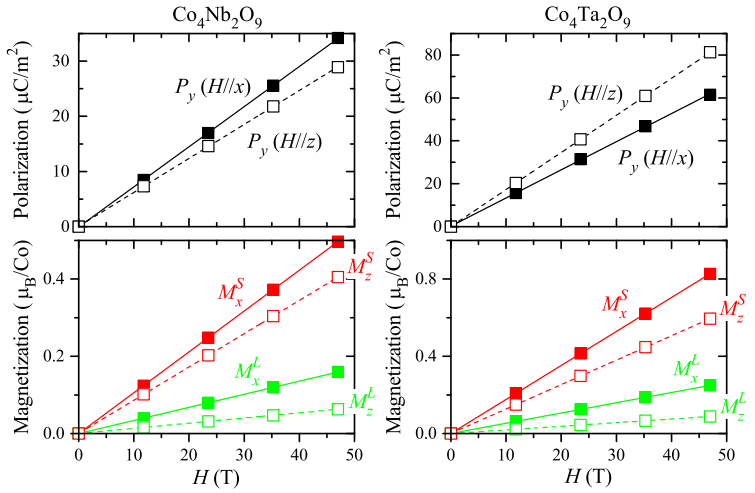

FIG. 12. (Color online) Nonvanishing components of electric polarization (P) and the net spin (M^S) and orbital (M^L) magnetization as obtained in the model Hartree-Fock calculations for the $\boldsymbol{G}_2$ state in the magnetic field being parallel to either x or z axes.

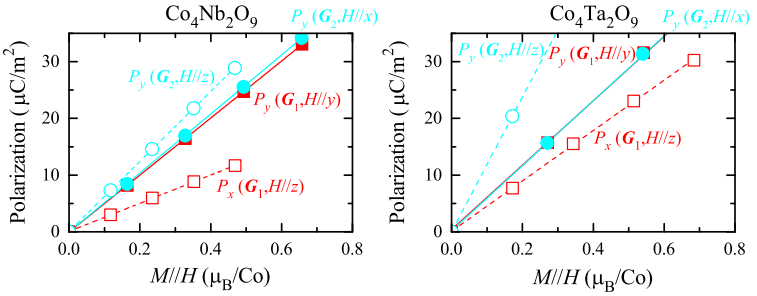

FIG. 13. Electric polarization versus total (spin plus orbital) net magnetization as obtained in the model Hartree-Fock calculations for different directions of the magnetic field in the states $\boldsymbol{G}_1$ and $\boldsymbol{G}_2$.

for a given magnetic field H, P_y is larger in $Co_4Ta_2O_9$ only because this field induces larger net magnetization. Another factor, which further increases P_x and P_y (for $\boldsymbol{G}_1$ and $\boldsymbol{G}_2$, respectively) in the case of $Co_4Ta_2O_9$, is smaller band gap (see Fig. 9). Note that in the atomic limit the electric polarization is inversely proportional to the splitting between the occupied and unoccupied atomic levels.[27] Since the band gap is formed between the states of the atoms Co(1) and Co(2), alternating along the z axis (see Fig. 3), this effect will be more important for $\boldsymbol{H}//z$.

The polarization, calculated for given values of the magnetic field, is substantially underestimated in comparison with the experimental data. However, this is mainly due to the overestimation of the exchange interactions in the low-energy model, which makes the magnetic structure harder than in the experiment. If one considers the slope P/M, which is less sensitive to the hardness of the magnetic structure, we will find a much better agreement with the experiment: for instance, for $\boldsymbol{H}//x$ or y, the theoretical P/M is about 50 $\mu C/(\mu_{\rm B} m^2)$ both for $Co_4Nb_2O_9$ and $Co_4Ta_2O_9$, which is comparable with the experimental value of about 100 $\mu C/(\mu_{\rm B} m^2)$.[7,10]

In the $P\overline{3}c1$ structure of $Co_4Nb_2O_9$ and $Co_4Ta_2O_9$, the are two inequivalent sublattices of the Co sites, each of which can exhibit the ME effect: namely, the external magnetic field breaks the inversion symmetry in each of the two sublattices and, therefore, the total polarization is the superposition of such effects in the two sublattices (as well as the interaction between the sublattices). In order to evaluate the contribution of the magnetic inversion symmetry breaking in each of the sublattices, we apply the nonuniform magnetic field, acting on either Co(1) or Co(2) sublattices and evaluate the electric polarization. The results of these calculations for the state $\boldsymbol{G}_1$ are presented in Fig. 14 (the results for the state $\boldsymbol{G}_2$ are very similar and not shown here). The most interesting aspect of these calculations is that the electric polarization induced by magnetic field in the Co(1) and Co(2) sublattices is of the opposite sign. For $Co_4Nb_2O_9$, the sum of these two contributions is very close to the total polarization, calculated in the uniform magnetic field. The small deviation in the case of $Co_4Ta_2O_9$ is caused by the additional deformation of the magnetic structure in the nonuniform field as well as stronger inter-sublattice interaction due to the smaller band gap (Fig. 9). Thus, we find a strong cancelation of contributions of the magnetic sublattices Co(1) or Co(2) to the electric polarization. In the $\boldsymbol{G}_1$ state, this cancelation is especially strong for $\boldsymbol{H}//z$, which explains smaller value of the induced polarization than for $\boldsymbol{H}//y$. In principle, such effect offers a possibility to control and reverse the electric polarization.

IV. DISCUSSIONS AND CONCLUSIONS

We have clarified the origin of ME effect in the centrosymmetric trigonal systems $Co_4Nb_2O_9$ and $Co_4Ta_2O_9$. Both compounds form the AFM structure, in which the FM chains of Co atoms are antiferromagnetically coupled in the hexagonal plane. The magne-

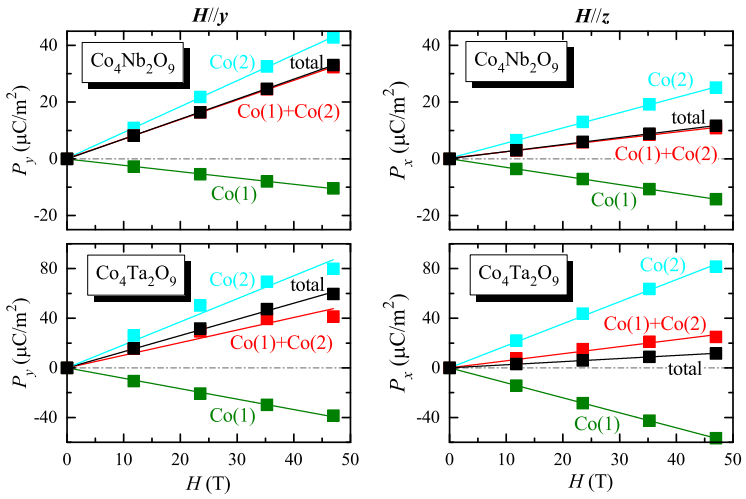

FIG. 14. (Color online) Electric polarization in $Co_4Nb_2O_9$ and $Co_4Ta_2O_9$ as obtained in the model Hartree-Fock calculations for the $\boldsymbol{G}_1$ state when the magnetic field was applied to either Co(1) or Co(2) sublattice. The sum of these two contributions is denoted as 'Co(1)+Co(2)', and 'total' is the polarization in the uniform magnetic field applied simultaneously to both magnetic sublattices.

tocrystalline anisotropy tends to align the magnetic moments in the hexagonal plane, thus, lowering the original $P\overline{3}c1$ space group symmetry. Nevertheless, the magnetic alignment obeys the $\hat{I}\hat{T}$ symmetry, meaning that, in the ground state, these compounds exhibit neither the net magnetization nor the spontaneous polarization, but both of them can be induced by either electric or magnetic field, which breaks $\hat{I}\hat{T}$. In this sense, the situation is similar to the canonical ME compound Cr_2O_3.[2] The new aspect of $Co_4Nb_2O_9$ and $Co_4Ta_2O_9$ is the existence of two inequivalent Co sublattices, which contribute to the ME effect. We have found that these contributions are of the opposite signs and, therefore, partly compensate each other. Nevertheless, under certain conditions, this balance can be shifted in either way, thus, giving a possibility to control the direction and magnitude of the ME effect.

Summarizing results of our joint experimental and theoretical studies, we first note that, as far as magnetic properties are concerned, $Co_4Ta_2O_9$ seems to be softer than $Co_4Nb_2O_9$. Experimentally, it is clearly observed in the behavior of Néel and absolute values of Weiss temperatures, which are systematically lower in $Co_4Ta_2O_9$. Moreover, the direct comparison of the behavior of magnetization, which was reported in Refs. 9 and 10, suggests that the AFM structure can be easier deformed by the magnetic field to induce larger net magne-

tization in $Co_4Ta_2O_9$. These experimental data were qualitatively explained by theoretical calculations of interatomic exchange interactions, which are generally weaker in $Co_4Ta_2O_9$. This behavior in turn nicely correlates with the details of the electronic structure calculations of $Co_4Nb_2O_9$ and $Co_4Ta_2O_9$. The quantitative differences between the theory and experiment are related to the fact that the theoretical calculations were performed using minimal effective Hubbard-type model, constructed only for the Co3d states, which overestimates the tendencies towards the antiferromagnetism.[23,24]

From the viewpoint of the minimal electron model considered in the present work the main factor controlling the behavior of the polarization in $Co_4Nb_2O_9$ and $Co_4Ta_2O_9$ should be the softness of the magnetic structure and its ability to be deformed by the external magnetic filed. Then, we would expect that the application of the magnetic filed should induce larger polarization in magnetically softer $Co_4Ta_2O_9$ than in $Co_4Nb_2O_9$, as it was indeed obtained in our theoretical calculations. However, there is number of experimental data, which suggest the opposite tendency. Particularly, the dielectric response to the magnetic field near T_N, studied in the present work, is weaker in $Co_4Ta_2O_9$. Moreover, the experimental polarization, induced for a given magnetic field is systematically smaller in $Co_4Ta_2O_9$ than in $Co_4Nb_2O_9$.[9,10] Yet, the experimental situation is somewhat controversial because the first direct measurements of the ME susceptibility suggested the opposite tendency:[3] the susceptibility was systematically larger in $Co_4Ta_2O_9$, but exhibited some nonmonotonous behavior as the function of temperature. Thus, we believe that this issue requires a more systematic study and it would be important, for instance, to measure directly the ME susceptibility for the single crystalline sample.

Below, we discuss some factors, which have not been taken into account by our theoretical model and which can alter some of our conclusions and also affect the comparison with the experimental data.

(i) The magnetostriction effect in the ordered magnetic phase can play an important role. In our theoretical calculations we used the experimental structure parameters, measured around the room temperature: $T = 297$ K for $Co_4Nb_2O_9$ and $T = 298$ K for $Co_4Ta_2O_9$.[15,16] These parameters do not take into account some possible change of the crystal structure, which may occur below T_N. Indeed, since the magnetic alignment in the hexagonal plane lowers the original $P\overline{3}c1$ symmetry, it is reasonable to expect also some changes in the crystal structure, which adjust to the change of the magnetic structure. In this sense, it is somewhat

surprising that no structural phase transition has been observed in the experiment.[7] Nevertheless, some structural change below T_N cannot be completely ruled out because of the following observations. First, the dielectric constant in $Co_4Nb_2O_9$ exhibits a clear upturn below T_N, even without magnetic field, as it was observed in Ref. 12 and also confirmed by our measurements. As it was argued in Ref. 12, this change can be of magnetostrictive origin. Second, the electric polarization induced by the magnetic field in $Co_4Nb_2O_9$ has a pronounced off-diagonal component.[7] This finding is inconsistent with the $P\overline{3}c1$ symmetry, according to which the polarization should be parallel to the y axis for $\boldsymbol{H}//x$ or y (depending on the magnetic state), or parallel to either y or x axis when $\boldsymbol{H}//z$, but there should be no off-diagonal components of the polarization in the xy plane.

(ii) Another important issue is the possible change of the magnetic structure, which can be induced, for instance, by pooling electric field used in some of the experiments (e.g., in Ref. 7) or some other factors. How robust is the obtained AFM ground state and whether $Co_4Nb_2O_9$ and $Co_4Ta_2O_9$ are the conventional ME systems? Or, can these compounds under certain conditions become type-II multiferroics, where the onset of electric polarization is triggered by some massive changes in the magnetic structure, which breaks spontaneously the inversion symmetry?[1] The above scenario looks quite feasible taking into account the complexity of magnetic interactions (Fig. 10), many of which are antiferromagnetic, not necessarily restricted by the nearest neighbors, and competing with each other. On many occasions such behavior is responsible for the type-II multiferroism.[1,28] In order to explore this possibility in $Co_4Nb_2O_9$ and $Co_4Ta_2O_9$ we have performed self-consistent HF spin-spiral calculations without the SO coupling, based on the generalized Bloch theorem.[29] The results are presented in Fig. 15. In this case, $\boldsymbol{q} = 0$ correspond to the ground-state AFM alignment, which is deformed for finite spin-spiral propagation vectors $\boldsymbol{q}$. For each value of $\boldsymbol{q}$, the magnetic moments in the xy plane were allowed to freely relax in order to minimize the total energy of the system. For $\boldsymbol{q}//z$ the dependence $E(q)$ is very flat (contrary to $\boldsymbol{q}//x$) when the energy change remains less than 1 meV/Co even for relatively large $q = |\boldsymbol{q}|$. In such situation the ground state is still $\boldsymbol{q} = 0$. However, any perturbation of the magnetic system, linear in $\boldsymbol{q}$, can induce the transition to a noncollinear state with the broken inversion symmetry, which will further affect the behavior of electric polarization. For instance, such transition can be caused by the electric field, leading to the off-centrosymmetric atomic displacements and appearance of Dzyaloshinskii-Moriya interactions,[30] connecting different

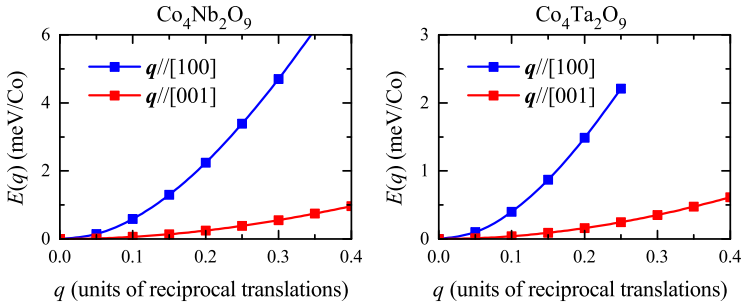

FIG. 15. (Color online) Dependence of the total energy on the spin-spiral vector q as obtained in the mean-field Hartree-Fock calculations for $Co_4Nb_2O_9$ and $Co_4Ta_2O_9$.

unit cells.

Acknowledgements. The work of IVS is partly supported by the grant of Russian Science Foundation (project No. 14-12-00306). TVK was supported by Grant-in-Aid for Scientific Research C 26400323 from JSPS.

---

* SOLOVYEV.Igor@nims.go.jp

[1] T. Kimura, Annu. Rev. Mater. Res. **37**, 387 (2007); S.-W. Cheong and M. Mostovoy, Nature Materials **6**, 13 (2007); D. Khomskii, Physics **2**, 20 (2009); Y. Tokura and S. Seki, Adv. Mater. **22**, 1554 (2010).

[2] I. E. Dzyaloshinskii, J. Exp. Theor. Phys. **37**, 881 (1959).

[3] E. Fischer, G. Gorodetsky, and R. M. Hornreich, Solid State Comm. **10**, 1127 (1972).

[4] E. F. Bertaut, L. Corliss, F. Forrat, R. Aleonard, R. Pauthenet, J. Phys. Chem. Solids **21**, 234 (1961).

[5] B. Schwarz, D. Kraft, R. Theissmann, H. Ehrenberg, J. Magn. Magn. Mater. **322**, L1 (2010).

[6] Y. Cao, Y. Yang, M. Xiang, Z. Feng, B. Kang, J. Zhang, W. Ren, and S. Cao, J. Crystal Growth **420**, 90 (2015).

[7] N. D. Khanh, N. Abe, H. Sagayama, A. Nakao, T. Hanashima, R. Kiyanagi, Y. Tokunaga, and T. Arima, Phys. Rev. B **93**, 075117 (2016).

[8] T. Kolodiazhnyi, H. Sakurai, and N. Vittayakorn, Appl. Phys. Lett. **99**, 132906 (2011).

[9] Y. Fang, Y. Q. Song, W. P. Zhou, R. Zhao, R. J. Tang, H. Yang, L. Y. Lv, S. G. Yang, D. H.

Wang, and Y. W. Du, Sci. Rep. **4**, 3860 (2014).

[10] Y. Fang, S. Yan, L. Zhang, Z. Han, B. Qian, D. Wang, and Y. Du, J. Am. Ceram. Soc. **98**, 2005 (2015).

[11] Y. Fang, W. P. Zhou, S. M. Yan, R. Bai, Z. H. Qian, Q. Y. Xu, D. H. Wang, and Y. W. Du, J. Appl. Phys. **117**, 17B712 (2015).

[12] Y. M. Xie, C. S.Lin, H. Zhang, and W. D. Cheng, AIP Advances **6**, 045006 (2016).

[13] V. Petricek, M. Dusek, and L. Palatinus, Z. Kristallogr. **229**, 345 (2014).

[14] N. Mufti, G. R. Blake, M. Mostovoy, S. Riyadi, A. A. Nugroho, and T. T. M. Palstra, Phys. Rev. B. **83**, 104416 (2011).

[15] M. A. R. Castellanos, S. Bernès, and M. Vega-González, Acta Cryst. E **62**, i117 (2006).

[16] W. Wong-Ng, H. F. McMurdie, B. Paretzkin, C. R. Hubbard, A. L. Dragoo, and J. M. Stewart, Powder diffraction **2**, 106 (1987).

[17] I. V. Solovyev, J. Phys.: Condens. Matter **20**, 293201 (2008).

[18] N. Marzari, A. A. Mostofi, J. R. Yates, I. Souza, and D. Vanderbilt, Rev. Mod. Phys. **84**, 1419 (2012).

[19] O. Gunnarsson, O. Jepsen, and O. K. Andersen, Phys. Rev. B **27**, 7144 (1983).

[20] F. Aryasetiawan, M. Imada, A. Georges, G. Kotliar, S. Biermann, and A. I. Lichtenstein, Phys. Rev. B **70**, 195104 (2004).

[21] All parameetrs of the model Hamiltonian are available upon request.

[22] A. I. Liechtenstein, M. I. Katsnelson, V. P. Antropov, and V. A. Gubanov, J. Magn. Magn. Matter. **67**, 65 (1987).

[23] I. V. Solovyev, Phys. Rev. B **91**, 224423 (2015).

[24] I. V. Solovyev, I. V. Kashin, and V. V. Mazurenko, Phys. Rev. B **92**, 144407 (2015).

[25] K. I. Kugel and D. I. Khomskii, Sov. Phys. Usp. **25**, 231 (1982).

[26] R. D. King-Smith and D. Vanderbilt, Phys. Rev. B **47**, 1651 (1993); D. Vanderbilt and R. D. King-Smith, *ibid.* **48**, 4442 (1993); R. Resta, J. Phys.: Condens. Matter **22**, 123201 (2010).

[27] I. V. Solovyev and S. A. Nikolaev, Phys. Rev. B **90**, 184425 (2014).

[28] I. V. Solovyev and Z. V. Pchelkina, Phys. Rev. B **82**, 094425 (2010); **90**, 179909(E) (2014). I. V. Solovyev, Phys. Rev. B **83**, 054404 (2011); **90**, 179910(E) (2014).

[29] L. M. Sandratskii, Adv. Phys. **47**, 1 (1998).

[30] I. Dzyaloshinsky, J. Chem. Phys. Solids **4**, 241 (1958); T. Moriya, Phys. Rev. **120**, 91 (1960).